Advanced Materials & Sustainable Manufacturing

SCIEPublish

Supporting Information

Te Substitution-Induced Structural Evolution and Thermoelectric Properties of Quasi-1D BiSeI

Zhiyao Zhang [1,2], Zuyong Feng [1,*] and Jian Zhou [2,*]

[1] School of Physics and Optoelectronic Engineering, Guangdong University of Technology, Guangzhou 510006, China; zhiyaozhang08@gmail.com (Z.Z.)

[2] School of Materials Science and Engineering, State Key Laboratory of Optoelectronic and Technology, Key Laboratory for Polymeric Composite and Functional Materials of Ministry of Education, Guangzhou Key Laboratory of Flexible Electronic Materials and Wearable Devices, Laboratory of Advanced Electronics and Fiber Materials, Sun Yat-sen University, Guangzhou 510275, China

* Corresponding author. E-mail: fengzuyong@gdut.edu.cn (Z.F.); zhouj296@mail.sysu.edu.cn (J.Z.)

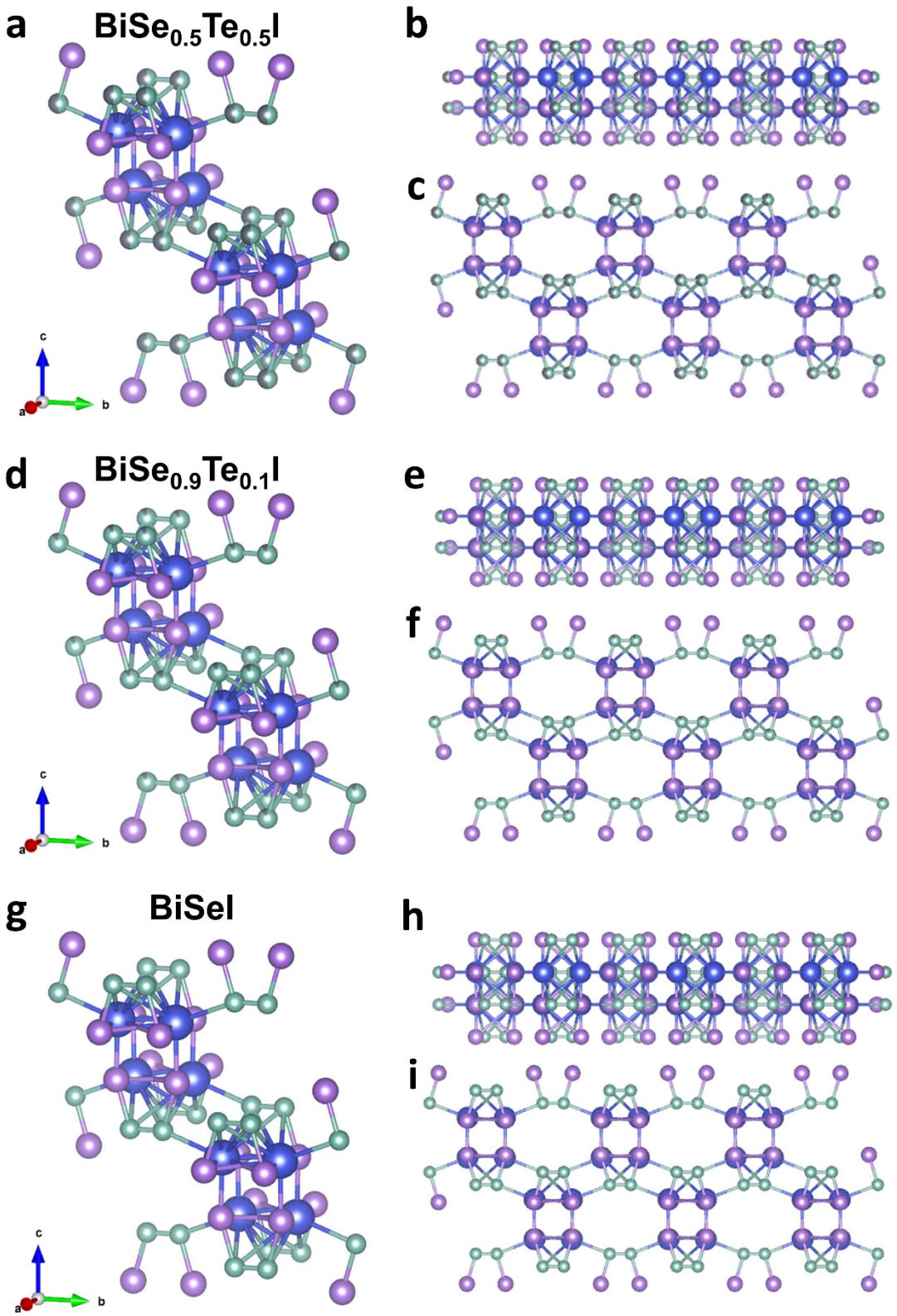

Figure S1. Multi-view comparison of crystal structures in the $BiSe_{1-x}Te_xI$ series. (**a**–**c**) $BiSe_{0.5}Te_{0.5}I$: (**a**) three-dimensional perspective; (**b**) projection along a showing the layered stacking and coordination polyhedra arrangement; (**c**) top view along c revealing the periodic atomic network within the ab plane. (**d**–**f**) $BiSe_{0.9}Te_{0.1}I$: (**d**) three-dimensional perspective; (**e**) projection along a; (**f**) top view along c. Relative to the higher-Te sample, the overall framework is retained with isovalent occupation of the (Se/Te) sites. (**g**–**i**) BiSeI (undoped reference): (**g**) three-dimensional perspective; (**h**) projection along a; (**i**) top view along c, clearly exhibiting the quasi-one-dimensional Bi–Se–I framework that provides substitutional sites for Te. (Uniform color scheme and crystallographic-direction arrows are used as in Figure 1: Bi-blue, I-purple, Te-gray, Se-cyan).

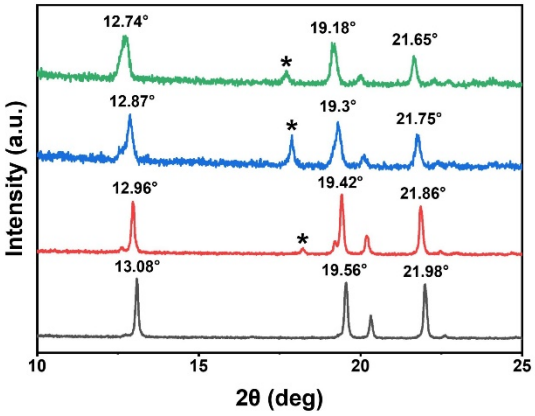

Figure S2. Enlarged powder XRD patterns (2θ = 10–25°) of BiSeI and Te-substituted $BiSe_{1-x}Te_xI$ (x = 0, 0.1, 0.3, 0.5). Representative reflections show a systematic shift toward lower 2θ with increasing Te content, indicating lattice expansion due to Te-for-Se substitution. Weak extra reflections marked with asterisks (*) correspond to trace secondary phases.

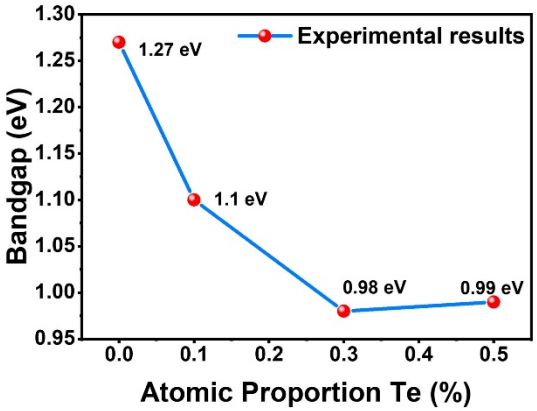

Figure S3. Band gap variation of $BiSe_{1-x}Te_xI$ (x = 0, 0.1, 0.3, 0.5). The optical band gap decreases progressively from 1.27 eV (x = 0) to 1.10 eV (x = 0.1) and 0.98 eV (x = 0.3), then increases slightly to 0.99 eV at x = 0.5. This non-monotonic trend reflects the competing effects of Te substitution: lattice expansion and electronic-structure modulation dominate at moderate doping, whereas excess Te introduces disorder that partially counteracts band gap narrowing.

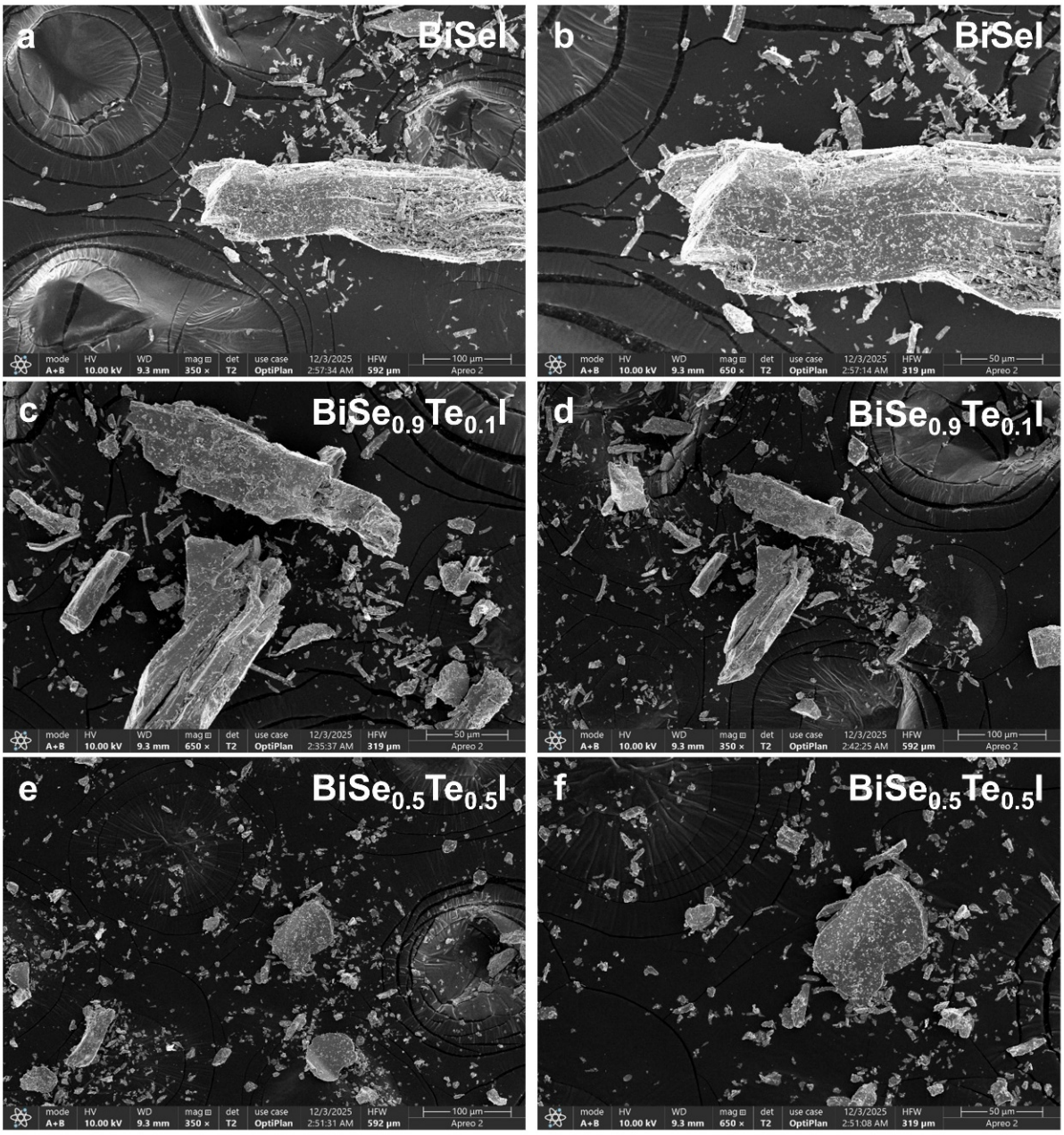

Figure S4. SEM images of BiSeI-based powders with different Te contents. (**a**,**b**) Low- and high-magnification images of BiSeI powder, showing belt-like particles. (**c**,**d**) $BiSe_{0.9}Te_{0.1}I$ powder exhibiting partially fractured, plate-like particles. (**e**,**f**) $BiSe_{0.5}Te_{0.5}I$ powder composed of highly fragmented, irregular grains, indicating that increasing Te substitution gradually destroys the original belt-like morphology.

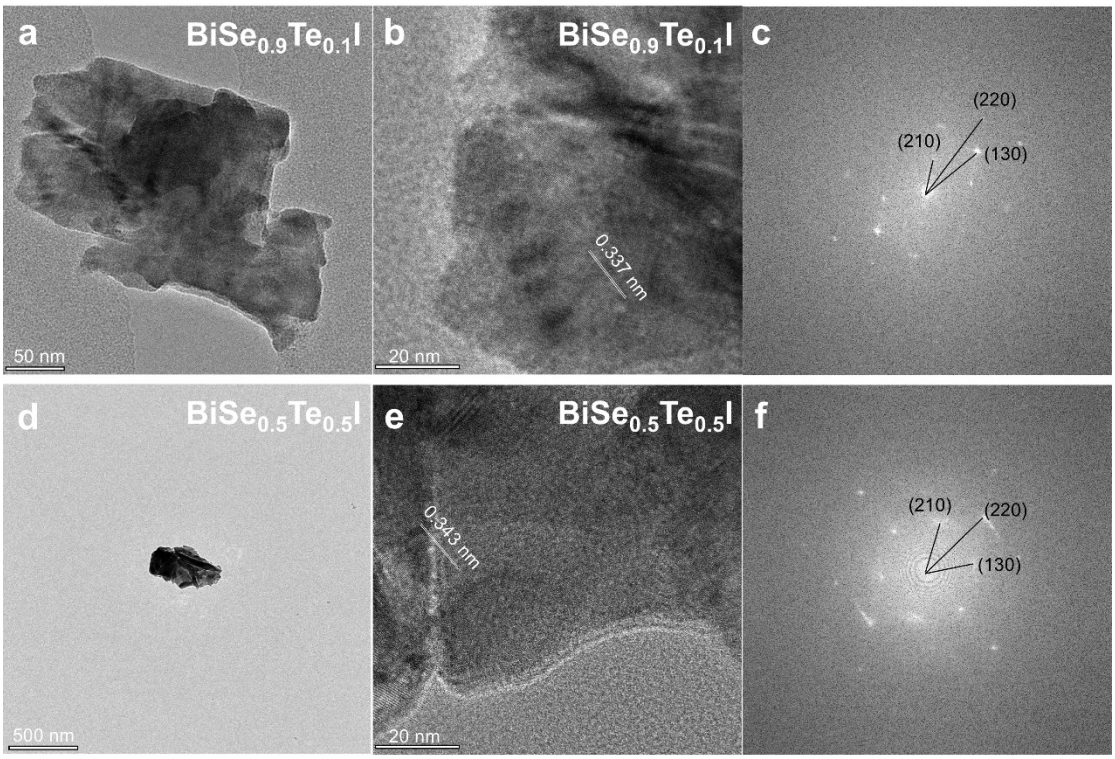

Figure S5. TEM characterization of Te-doped BiSeI powders. (**a**,**d**) Low-magnification TEM images of $BiSe_{0.9}Te_{0.1}I$ and $BiSe_{0.5}Te_{0.5}I$ powders, showing flake-like particles. (**b**,**e**) High-resolution TEM (HRTEM) images displaying clear lattice fringes with interplanar spacings of ~0.337 and ~0.343 nm, respectively, confirm the good crystallinity of both powders. (**c**,**f**) Fast-Fourier-transform (FFT) processed selected-area electron diffraction (SAED) patterns derived from the HRTEM images, in which the diffraction spots can be indexed to the (220), (130), and (210) planes of the BiSeI-type phase, indicating that Te substitution does not alter the basic crystal structure.

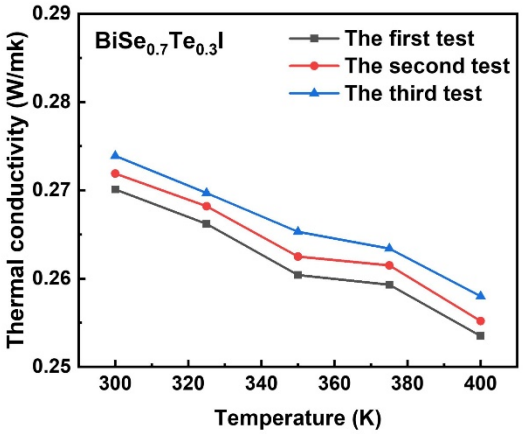

Figure S6. Temperature-dependent thermal conductivity of $BiSe_{0.7}Te_{0.3}I$. Thermal conductivity (κ) was measured from 300–400 K in three independent tests, each showing a monotonic decrease with temperature. The values used in the manuscript are the averages of the three tests at each temperature.

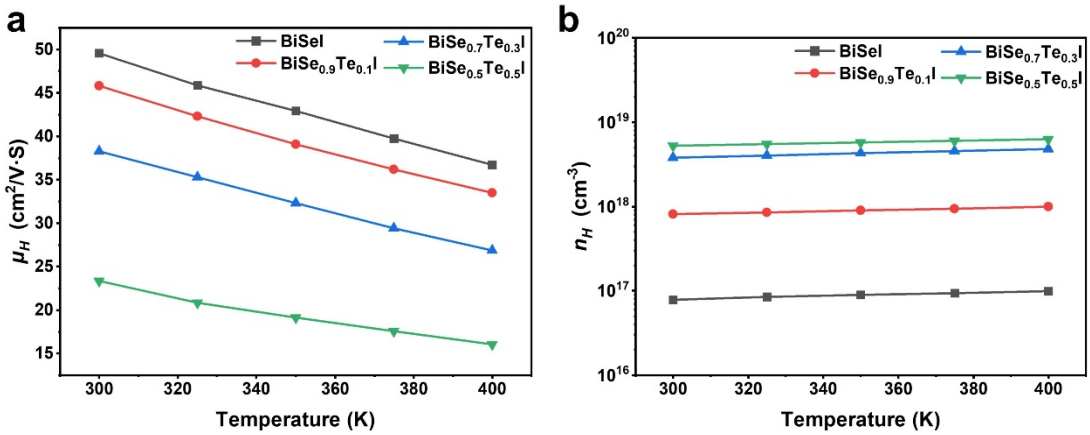

Figure S7. Temperature-dependent Hall transport parameters of $BiSe_{1-x}Te_xI$ (x = 0, 0.1, 0.3, 0.5) measured in the 300–400 K range. (**a**) Hall mobility, μ_H. (**b**) Hall carrier concentration, n_H (plotted on a logarithmic scale). All samples exhibit *n*-type transport (consistent with negative Seebeck coefficients), and Te substitution leads to a pronounced increase in n_H while μ_H decreases with increasing temperature.

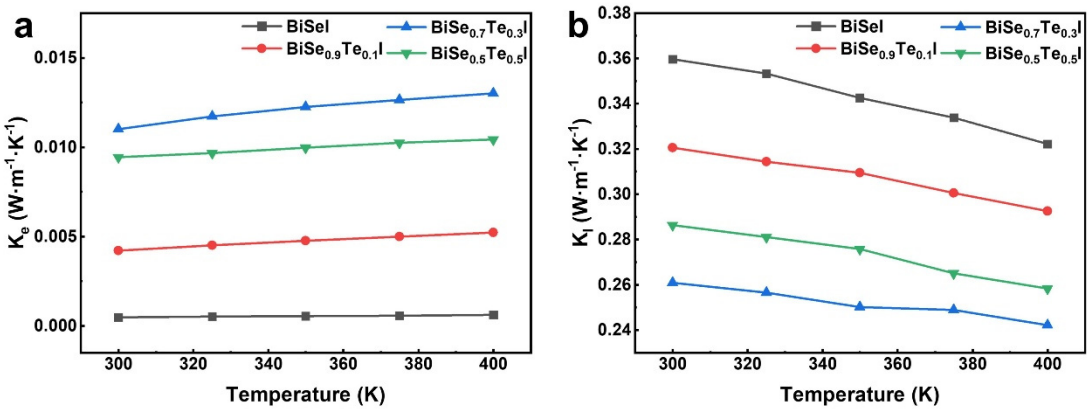

Figure S8. Temperature dependence of the separated thermal conductivity components for $BiSe_{1-x}Te_xI$ (x = 0, 0.1, 0.3, 0.5) in the range of 300–400 K. (**a**) Electronic thermal conductivity, κ_e, calculated using the Wiedemann–Franz relation $\kappa_e = L\sigma T$ with a Seebeck-dependent Lorenz number *L*. (**b**) Lattice thermal conductivity, κ_l, obtained by $\kappa_l = \kappa - \kappa_e$. The results indicate that κ_e contributes only a minor fraction of κ, and the reduction of thermal conductivity upon Te substitution is dominated by the suppression of κ_l due to enhanced phonon scattering.

Table S1. Elemental compositions of $BiSe_{1-x}Te_xI$ powders determined by SEM–EDS.

Sample	Element (at.%)			
	Bi	Se	Te	I
BiSeI	32.1	33.0	0	34.9
$BiSe_{0.9}Te_{0.1}I$	32.6	28.3	4.4	34.7
$BiSe_{0.7}Te_{0.3}I$	31.7	24.6	9.7	34.0
$BiSe_{0.5}Te_{0.5}I$	31.6	17.6	16.5	34.3

at.% represents the atomic percent. The compositions were obtained from SEM-EDS measurements and normalized to 100 at.% for each sample.

Table S2. Ratio of electronic thermal conductivity to total thermal conductivity (κ_e/κ, %) for $BiSe_{1-x}Te_xI$ (x = 0, 0.1, 0.3, 0.5) in the temperature range of 300–400 K.

T (K)	BiSeI	$BiSe_{0.9}Te_{0.1}I$	$BiSe_{0.7}Te_{0.3}I$	$BiSe_{0.5}Te_{0.5}I$
300	0.13%	1.30%	4.05%	3.19%
325	0.15%	1.41%	4.37%	3.32%
350	0.16%	1.51%	4.67%	3.49%
375	0.17%	1.64%	4.83%	3.72%
400	0.19%	1.76%	5.10%	3.88%

Here, κ_e was calculated using the Wiedemann–Franz relation ($\kappa_e = L\sigma T$), where the Lorenz number L was estimated from the Seebeck coefficient using L (10^{-8} W·Ω·K^{-2}) = 1.5 + exp(−|S|/116). The lattice contribution was obtained by $\kappa_l = \kappa - \kappa_e$.